Chapter 14

THE SMELTING OF COPPER-NICKEL CONCENTRATES IN AN ELECTRIC FURNACE

Roger C. Urquhart,
Quebec Iron and Titanium Corporation,
P.O. Box 40,
Sorel,
QUEBEC,
Canada.

Myles S. Rennie,
National Institute for Metallurgy,
Private Bag 7,
AUCKLAND PARK,
South Africa.

Chris C. Rabey,
Anglo American Corporation,
P.O. Box 61587,
MARSHALLTOWN,
South Africa.

Introduction

Copper-nickel-sulphide ores mined in the Rustenburg district of South Africa are generally smelted in electric furnaces because of the high-temperature slag produced, the availability of cheap electric power, and the smaller pollution problems. Apart from melting, the functions of the electric furnace are to recover most of the matte content in the converter slag by physical and chemical interaction with the furnace bath and to provide adequate time for the optimum separation of matte and slag. Smooth, efficient operation will depend on fluid slags for settling, balanced by high resistivities to obtain adequate concentration and distribution of power by way of current heating. To obtain a greater understanding of the processes involved, an investigation was undertaken at Rustenburg Platinum Mines on the smelting of copper-nickel concentrates in a 19.5 MVA furnace with six in-line electrodes.

The matte- and slag-tapping temperatures, slag temperatures, slag analyses, electrical data, and electrode position were measured. Radioactive tracers were introduced into the slag, and quantitative results relating to the flow pattern within the furnace were obtained. These studies were augmented by scaled laboratory investigations relating to the determination of cell constants and current distribution within the furnace. Instantaneous field and power distribution plots were determined by use of an on-line mini-computer. The applicability of these results to furnace operation is discussed.

Furnace Investigations

Matte- and slag-tapping temperatures, slag temperatures, slag analyses, electrical data, electrode position, and the flow pattern of slag in the electric furnace were observed. The slag-tapping temperatures, as measured by a quick-immersion thermocouple, varied between 1340 and 1390°C over one 24-hour period, the variation

depending upon the/...

depending upon the slag volume in the furnace and the working power of the furnace. The matte-tapping temperature varied between 1150 and 1250°C over the same period. On a subsequent occasion, temperatures in the slag were measured at various positions, and these are shown in Figure 1. The temperature in the slag is highest near the electrode, and decreases slowly towards the matte layer. It can be seen that the temperature is very uniform over a large volume of the furnace.

Samples of slag were obtained from the furnace by the freezing of slag onto a steel probe inserted in the melt. A sample was obtained in the region of each electrode, and at the matte-tapping and slag-tapping ends of the furnace. The analyses of the slag samples in the region of the electrodes showed that the slag layer is very homogeneous in composition over its vertical height. The matte content of the slag was found to be highest near the slag-matte interface as a result of the lower temperature and consequently higher viscosity of this particular level of the slag layer. Samples taken from the tapping ends of the furnace and next to electrode No. 1 showed an increase in the concentration of chromium oxide in the slag from 0.4 to about 6 per cent Cr_2O_3 at the slag-matte interface. Mineralogical investigation of a slag sample obtained from this region revealed that the chromium oxide was present as chromite. The chromium oxide was shown to originate from the ore and not from the chromium-magnesite bricks used for the converter linings. This is a problem peculiar to copper-nickel ores mined in the Rustenburg area of the Bushveld Igneous Complex, also well known for its vast reserve of chromite ore. The increase in chromium oxide concentration at the slag-matte interface at both ends of the electric furnace is due to the lower temperatures and small amount of mixing in these regions, which are further from the electrodes. The chromium oxide-rich region, which is indicated in Figure 1, extends to electrode No. 1, whereas electrode No. 6 is not affected in the same way. The explanation for this phenomenon is the return of the molten converter slag to the front of the furnace. The converter slag, which is rich in FeO, reduces the electrical resistivity of the furnace slag in the region of electrode No. 1. As a result, electrode No. 1 tends to stay for longer periods at a higher position in the slag layer, dissipating less heat and causing less stirring near the slag-matte interface.

Radioactive Tracer Experiments

Slag analyses and temperature measurements on the electric furnace have indicated that the slag layer is well mixed. Tracer experiments, similar to those conducted on a reverberatory furnace used to smelt copper concentrates[2], were done to determine the flow pattern in the electric furnace. In the first test, irradiated sodium carbonate was introduced into the slag layer by way of the inspection port at the matte-tapping end of the furnace. Slag samples were collected over a few days from the slag stream at the slag-tapping end of the furnace, and the tracer concentration in the samples was determined. For the second tracer test, irradiated sodium glass was inserted into the slag next to electrode No. 4, and slag samples were again collected from the slag stream.

The estimated mean residence time for slag in the electric furnace

is derived from/...

Slag, %		Matte, %		Converter Slag, %		Pelletized Concentrate, %		Limestone, %	
MgO	14.92	Cu	8.88	CaO	0.65	Fe	16.39	CaO	46.41
CaO	16.68	Ni	15.1	MgO	0.67	Cu	2.13	MgO	0.55
FeO	18.01	Fe	42.1	Al_2O_3	1.16	Ni	4.16	SiO_2	10.89
Fe_2O_3	0.3	S	28.59	FeO	60.1	S	10.34	Al_2O_3	0.65
SiO_2	42.79	Cr	0.091	SiO_2	35.2	CaO	3.29	FeO	0.41
Cr_2O_3	0.39			Cr_2O_3	0.28	MgO	15.96		
Cu	0.058					Al_2O_3	3.29		
Ni	0.079					SiO_2	35.75		
S	0.34					Cr_2O_3	0.31		
						H_2O	6		

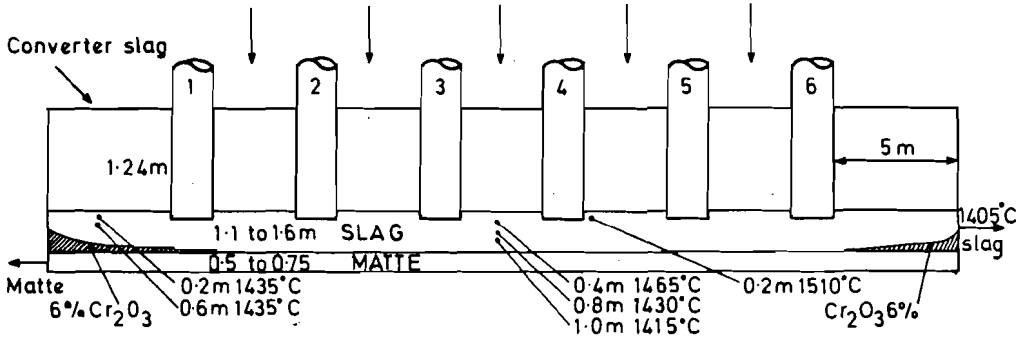

FIGURE 1 Inputs, outputs, and temperatures of the electric furnace studied

is derived from the volume of liquid slag in the vessel divided by the volumetric rate of flow.

$$\text{Estimated mean slag residence time } \bar{t} = \frac{292\ m^3}{9.4\ m^3/hr} = 31 \text{ hours.}$$

The residence-time distribution curves for the slag flow are given in Figure 2. In order to obtain valid comparison between the two tracer experiments, dimensionless concentration C was plotted against dimensionless time Θ where

$$C = \frac{\text{Concentration of tracer in the exit stream}}{\text{Total tracer concentration}}$$

$$\Theta = \frac{\text{Time}}{\text{Actual mean tracer residence time in the furnace } (\bar{t})}$$

One of the main sources of error in the evaluation of these experiments is the estimation of the volumetric rate of fluid flow. The total slag mass tapped from the two electric furnaces was recorded for each experimental period, from which an average volumetric flowrate based on data for the specific gravity of the slag at 1400°C[3] can be calculated. The instantaneous rate of flow will depend on the temperature of the slag, whether one or two tap holes are open, the hydrostatic head of slag above the tap hole, and the enthusiasn of the operator who is priming the tap holes. The volume of the slag in the furnace is also variable because of periodic imbalances between the amount of material added to and removed from the electric furnace.

The more apparent features of the normalized distribution curves are the low peak and the very long tail, indicative of a considerable degree of mixing within the furnace. The actual mean residence times for the tracer added at the matte-tapping end of the furnace (20.25 hours) and the tracer added next to electrode No. 4 (20.56 hours) are almost equal, which might imply that the furnace may be regarded as a large mixing tank with a bypass dead-volume region and a small plug-flow region. There is a strong similarity between the shape of these curves and those obtained by Themelis[4] (Figure 3) which are based on this simple model. The two curves describe the flow before and after a campaign of air and steam lancing to disperse a layer rich in chromite and magnesite near the slag-matte interface. Their curves fit the model well, since little charge is added to the last one-quarter to one-third of the reverberatory furnace, and it is quite conceivable that much of the active flow is mixing induced by the addition of converter slag in the first half of the furnace. However, the differences in heights of our peaks cannot be explained by this model, and a more realistic model would be the representation of the furnace as six mixing tanks around each electrode, with mass flow in both directions, as shown in Figure 3.

Comparison between the performance figures shows that the electric furnace exhibits a great deal more mixing than the reverberatory furnace, which is to be expected, because the large power concentration at the electrode tips (to be discussed later) gives rise to uneven temperature distribution, allowing considerable convection around the electrodes. This phenomenon is confirmed by the wear pattern of the electrode tips - similar to an indented bullet - and has been noticed previously.

Barth quotes the/...

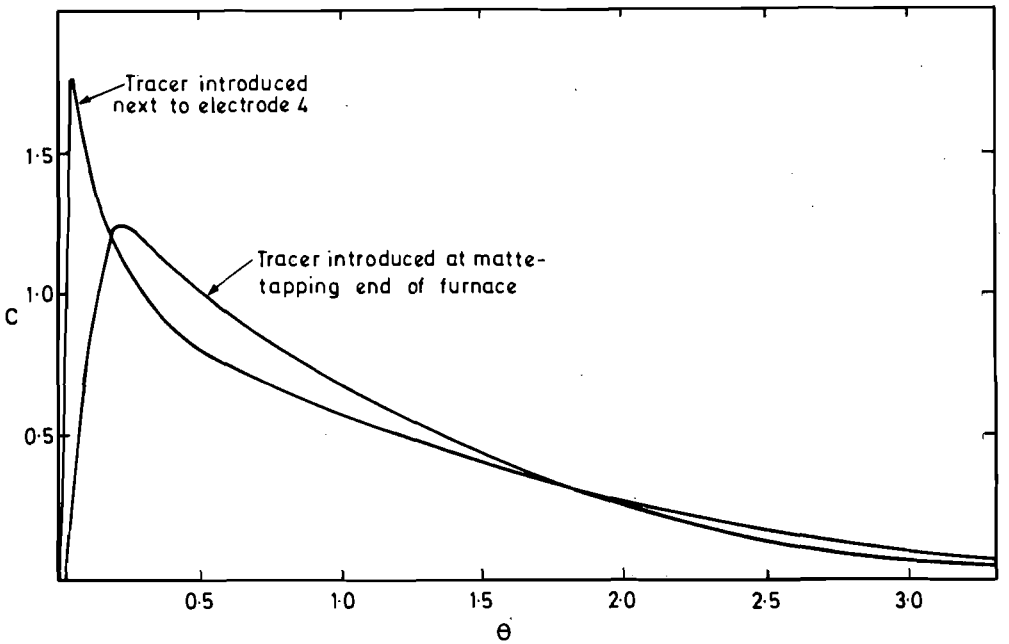

FIGURE 2 Normalized tracer distribution curves

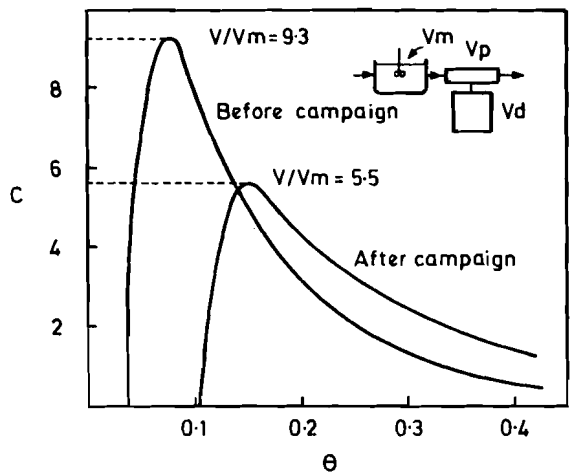

Distribution curves and flow model of the reverberatory furnace

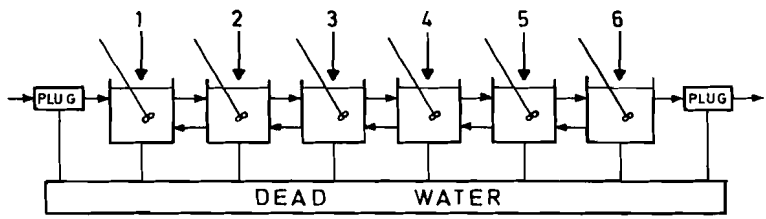

	Backmix	Plug flow	Dead water
% of total volume as	%	%	%
Electric-furnace slag	65.0	1.0	34
Reverberatory-furnace slag	10.4	3.5	86
Reverberatory-furnace slag (after blowing campaign)	18.2	7.8	74

FIGURE 3 Comparison of flow between electric and reverberatory furnaces

Barth[5] quotes the velocity of the slag moving from the electrode to the refractory wall as being 50 to 100 mm sec^{-1} for a 9 MVA three-electrode triangular furnace. Tseidler[6] maintains that, in practice, the rate of slag circulation in the upper area of the electrodes may reach 2 m sec^{-1}. This effect is probably heightened by electromagnetic agitation caused by the large alternating currents flowing through the slag. However, theoretical calculations imply that this effect is very small.

Laboratory Investigations

Sampling and temperature measurements of the furnace slag have shown it to be largely homogeneous. This homogeneity suggested the use of a room-temperature model to study the distribution of current and power in the bath of the electric furnace. The electrical conduction in the slag is assumed to be ohmic because, at the low current densities involved, arcing would not be possible, as shown by the work of Channon, et al.,[7] on ferrochromium slags. Also the waveforms observed on the plant were clean sinusoidal. Thus

$$R_s = \rho_s K \quad \ldots\ldots\ldots\ldots\ldots (1)$$

where R_s = slag resistance [ohm]

ρ_s = slag resistivity [ohm cm]

K = cell constant [cm^{-1}]

The dimensionless parameter for the scaling of the furnace will then be kD, where D is a length dimension and the electrode diameter is the one usually chosen. The pertinent electric-furnace dimensions were scaled down, as shown in Figure 4.

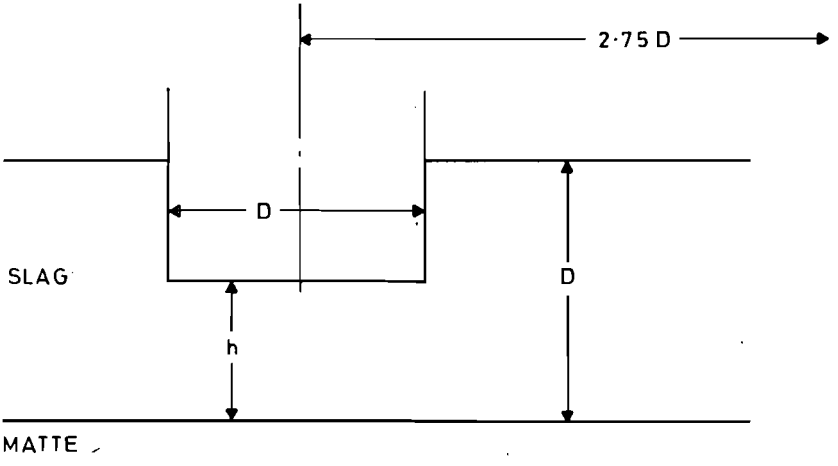

FIGURE 4 Electrode configuration in an electric furnace in terms of electrode diameter

Two models were/...

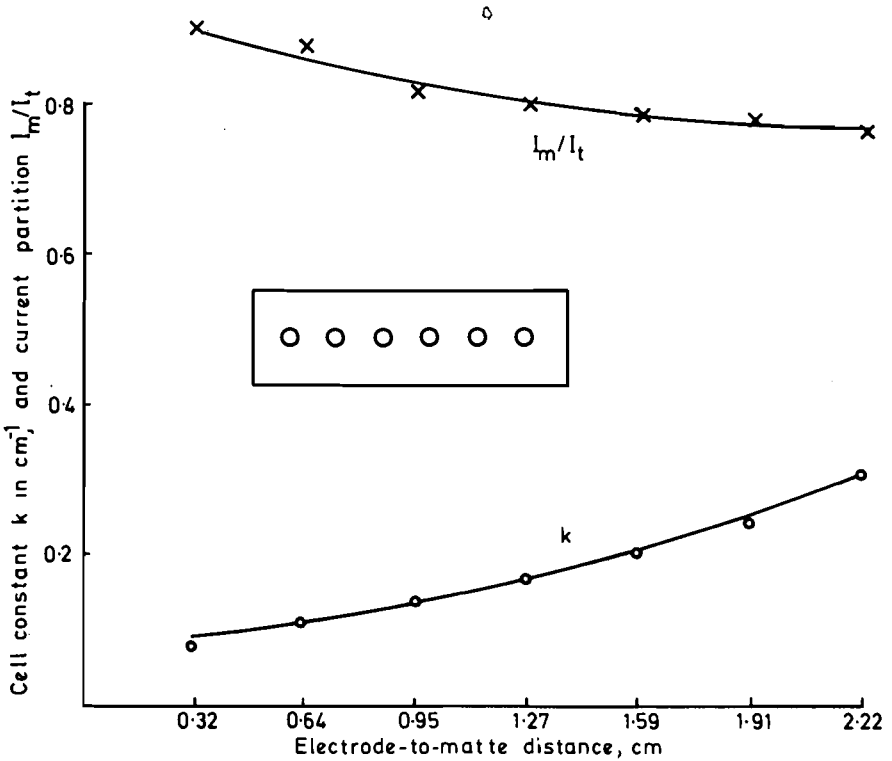

FIGURE 5 Cell constant and current partition for conduction from the electrodes in a six-in-line electric cell

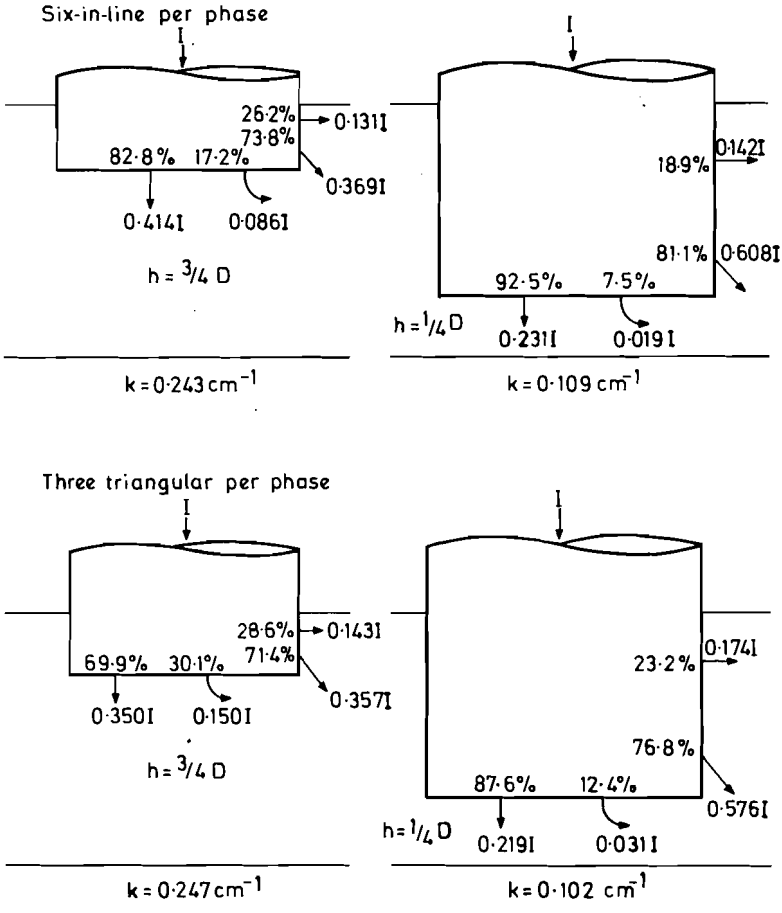

FIGURE 6 Current partition for a six-in-line compared with a three-triangular electric cell

Two models were constructed, a salt solution being used to simulate the slag layer and mercury, or a stainless-steel plate representing the low-resistivity matte layer. In the first model, it was possible to separate the mercury layer between the electrodes physically, and then reconnect the circuit through an ammeter, which enabled the partition of current flowing solely through the slag by way of the matte layer to be measured. The relative roles played by the electrode tips and sides can be determined by insulating either the sides or the tips. The measurements were made by use of a salt solution of known resistivity, and the cell constant was calculated according to equation (1).

The tests were done on a six-in-line and three-electrode configuration. The electrode diameters for the two different configurations were the same. The electrode separation for the six-in-line furnace was 2.75D, and for the three-electrode triangular furnace it was 2.6D. The three-electrode furnace would be designed for a lower power operation than the six-electrode furnace. Figure 5 illustrates the variation of cell constant k and the fraction of current flowing by way of the matte phase for different values of electrode penetration in the slag. Figure 6 summarizes the relative amount of current flow for the six-electrode in-line configuration and the three-electrode triangular configurations for the two extreme cases of electrode immersion in the slag. Although there will be an increase in slag resistivity towards the matte layer in the actual furnace, the results confirm Barth's[5] opinion that 2/3 to 3/4 of the total current flows by way of the matte phase.

In the second instance, a mini-computer was used to control the model and analyse the data. In this way, the field could be sampled at any desired instant of the current cycle over the three phases, and the position of the electrodes and voltage probe could be controlled by way of stepping motors. As shown in Figure 7, the inputs to the computer were the three-line currents, the six electrode-to-hearth voltages, and the potential, relative to the earth plate, of a voltage probe. Programmes were written to enable the computer to extract, process, and display data from the model. From the potential (ϕ), the electric field ($E = -\nabla\phi$), the current ($J = \sigma E$), and the power ($P \alpha E^2$) can be obtained.

Figure 8 shows the field plots for two electrodes on the surface at different depths in the X-Z plane and along the electrode axis in the X-Y plane. The magnitude and direction of the field is represented by vectors on the grid. It can be seen that the field on the surface is similar to that for two infinitely long parallel conductors - the Attwood expression[8]. From these figures, it was calculated that 70 per cent of the current flow is by way of the hearth. The two-dimensional plots in Figure 9 show the power distribution in the X-Z plane at different levels below the electrodes. The magnitude of E^2 has been plotted vertically across the whole plane. Figure 10 shows the power contours in the X-Y plane and the X-Z plane. Almost all the power has been dissipated within a sphere of radius equal to the electrode diameter, and most of the power is dissipated close to the electrode. This explains the higher temperatures measured next to the electrode. The temperature

profile does not/...

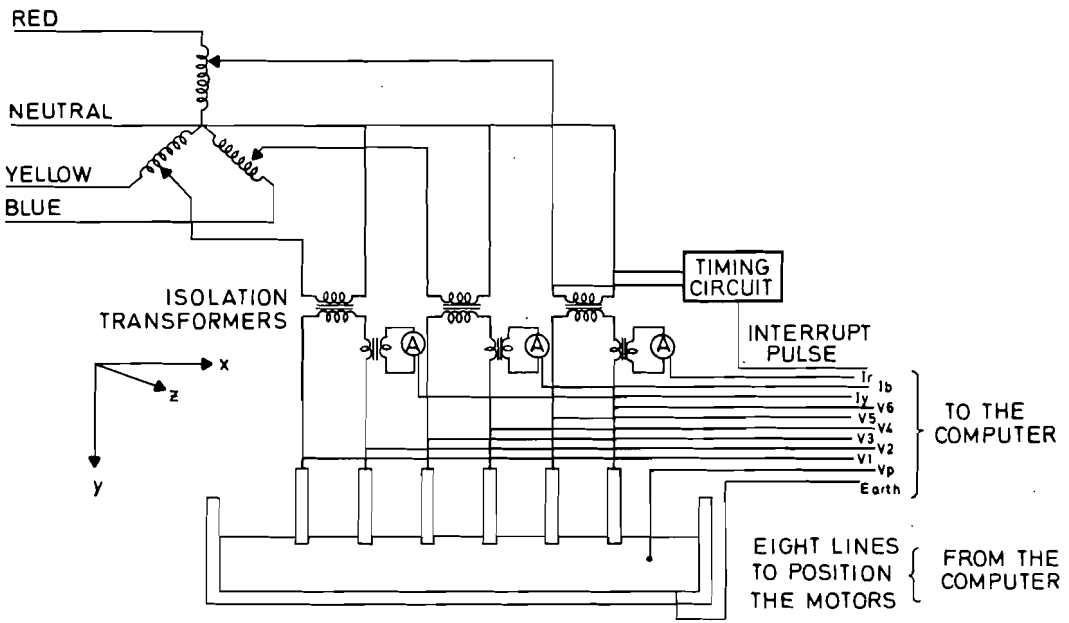

FIGURE 7 Electrical connections to the model

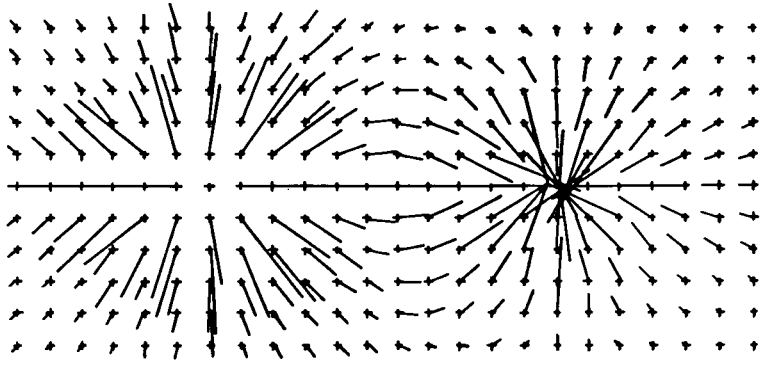

(a) X-Z Plane Y = 0.5 cms

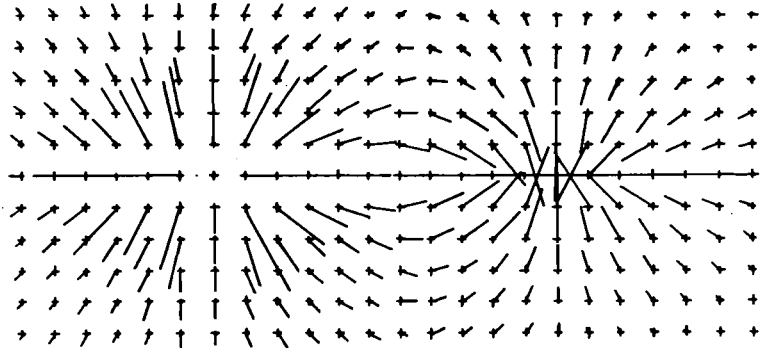

(b) X-Z Plane Y = 1.5 cms

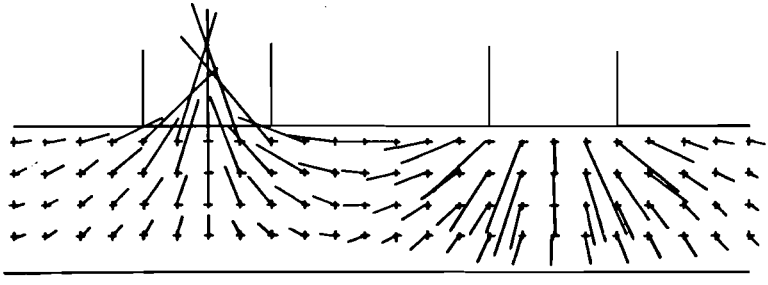

(c) X-Y Plane Z = 0.0 cms

FIGURE 8 Current distribution for two-electrode case

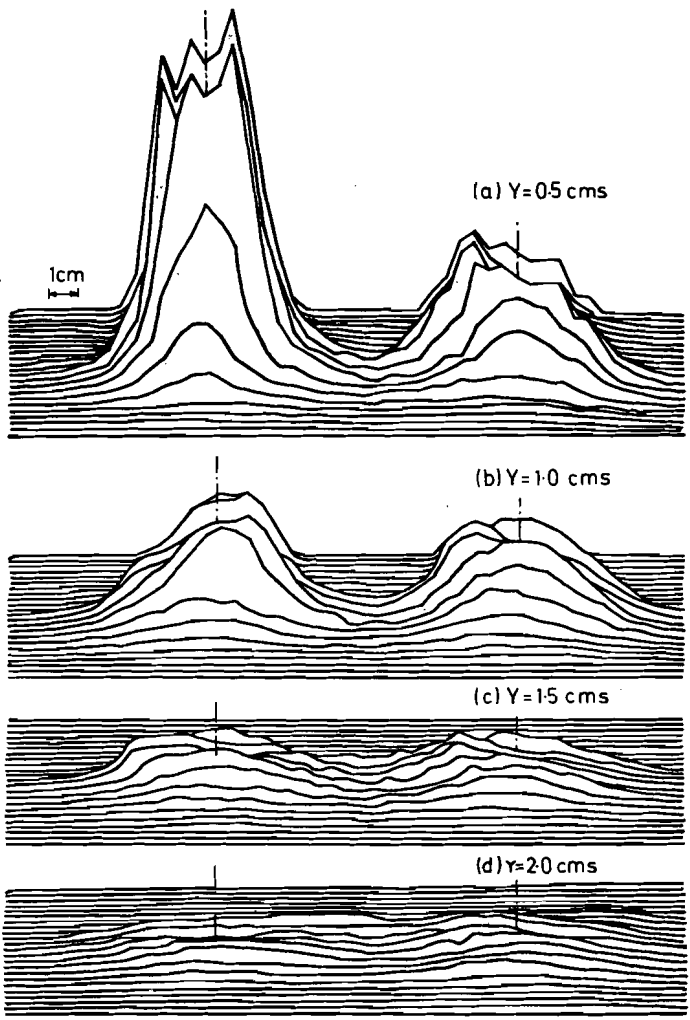

FIGURE 9 Power distribution over X-Z plane for two-electrode case

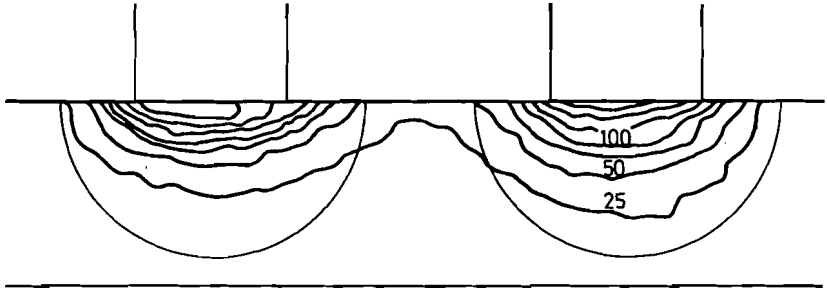

10 (a) x-y plane (z = 0 cm)

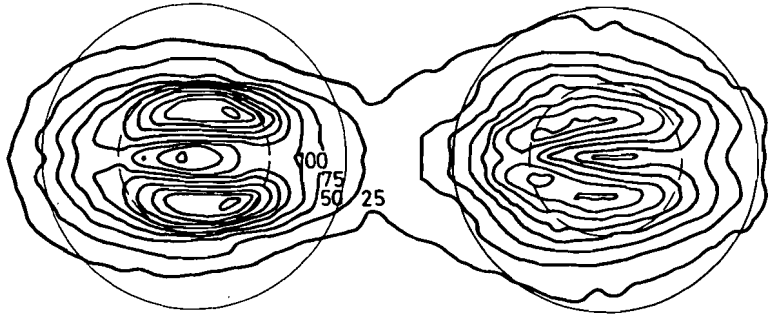

10(b) x-z plane (y = 0 cm)

FIGURE 10 Power contours around the electrodes

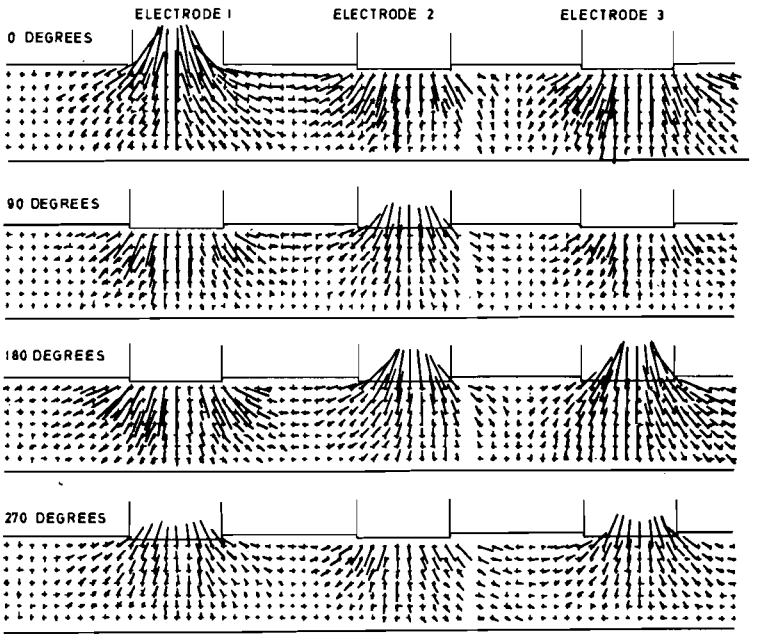

FIGURE 11 Fields in a three-phase furnace at different instants in the cycle

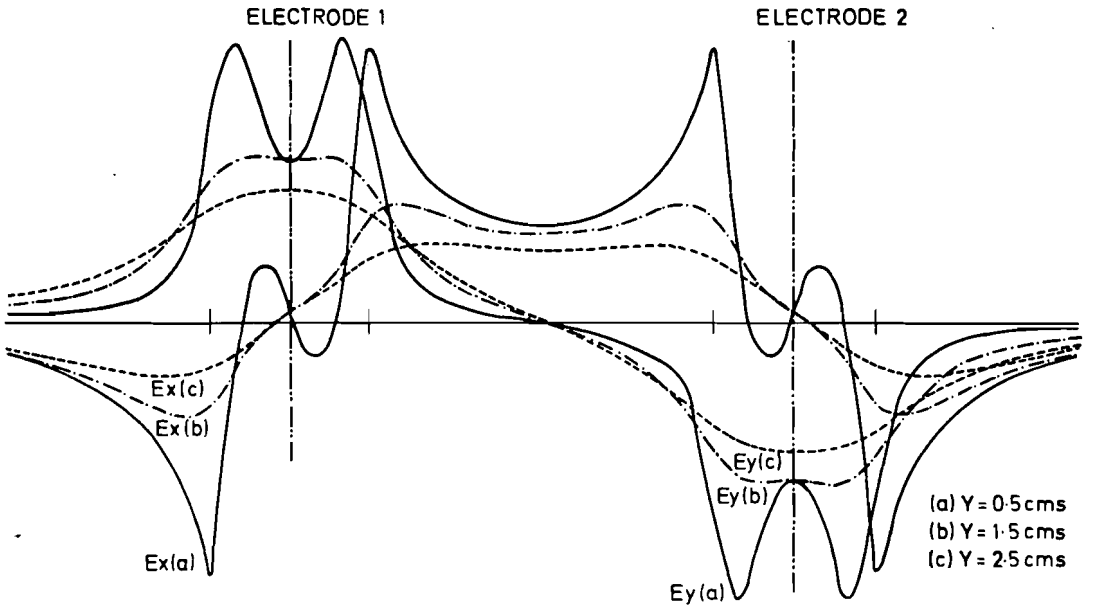

FIGURE 12 Components of current from field model.
Radius of electrode 60 cm

profile does not correspond to the power contours because of heat flow by way of convection and conduction. The field pattern throughout the furnace at different phase times is shown in Figure 11. The clear demarcation between out-of-phase fields can be clearly seen. At these low current densities there will be no effect due to the magnetic fields and, for relevant scaling up of the results, equations governing the fields in the furnace were derived directly from Maxwell's electromagnetic equations and solved for particular instances. Figure 12 shows the field components in the Z-Y plane which are similar to those obtained from the physical model. Increase of the current has little effect on the field distribution except in a small area around the electrode tip, where the non-uniform current input has an effect. This gives some confidence in the application of these field patterns to a real furnace.

Electric-Furnace Design

The information gained at the electric furnace and in the laboratory can be used as a basis for comment on certain aspects of electric-furnace design when the treatment of sulphide concentrates is involved. Once the power requirement has been established, the voltage current relationships that influence the electrode size and spacing, as well as the overall furnace dimensions have to be determined. For this to be done, the resistance in the slag bath must be predicted.

As pointed out earlier, the slag resistance R_s is given by its specific resistivity ρ_s times the cell constant k, i.e., $R_s = \rho_s k$. Values for the specific resistivity of the different slags involved have been determined by Mr Hejja[3]. The results of the model experiments should provide a guide towards a prediction of a cell constant.

The following are the more important equations available in the literature, and are based on the symbols given in Figure 13.

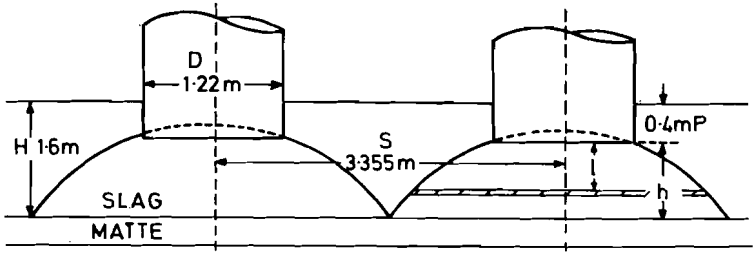

FIGURE 13 Electrode geometry in the electric furnace

Persson's equation/...

Persson's equation[8]:

$$k = \frac{1}{\frac{\pi P}{\ln\left[\frac{S}{D} + \sqrt{\frac{S^2}{D^2} - 1}\right]} + \pi D \left[1 + \frac{D}{2S} + \left(\frac{D}{2S}\right)^2 + \ldots\ldots\right]} \qquad (2)$$

Equation (2) represents a parallel combination of conduction between the sides of the electrodes (the logarithmic expression according to Attwood[9]) and conduction between the electrode tipe through the slag. Conduction by way of the matte layer has been ignored.

Hallvard - Nilsen's equation[10]:

$$k = \frac{0.3034}{D} \frac{\left(\frac{H + P}{D}\right)^{0.45}}{\left(\frac{P}{D}\right)^{0.24}} \qquad \ldots\ldots\ldots\ldots \qquad (3)$$

Equation (3) represents conduction from the electrode through the slag to the matte layer. Inter-electrode conduction between the electrode sides has been ignored.

Experimental measurement of the electric field patterns (Figure 11) has shown that the shape of the current path flowing from the tip of the electrode is approximated by a parabola. The electric field, and, therefore, the conduction paths, will be altered by the electrodes on either side, one in phase, and one 120° out of phase. The component that is out of phase will define the extension of the parabola to the mid-point between the two electrodes, and the component that is in phase can be approximated by the Attwood expression:

$$k = \frac{\Delta P}{\pi P} \ln\left[\frac{S}{D} + \sqrt{\left(\frac{S}{D}\right)^2 - 1}\right] \qquad \ldots\ldots\ldots\ldots \qquad (4)$$

for conduction between the sides of the electrodes. As sketched in Figure 13, the parabola of revolution is defined by the electrode diameter at the electrode tip, and one-half of the electrode separation at the slag-matte interface. The cell constant for the parabolic region of conduction is:

$$k = \frac{4h}{\pi(S^2 - D^2)} \ln\left[\frac{\ell + \Delta\ell + \frac{D^2 h}{S^2 - D^2}}{\ell + \frac{D^2 h}{S^2 - D^2}}\right] \qquad \ldots\ldots\ldots\ldots \qquad (5)$$

where ℓ is the distance of a conducting disc from the tip of the electrode and $\Delta\ell$ is its thickness. The advantage of this approach is that the expression can be integrated in steps. A stepwise integration is

necessary owing to/...

necessary owing to the change in temperature and therefore resistivity with depth in the slag layer.

A temperature profile based on the temperatures measured in the furnace was predicted. With the use of this temperature profile, and subdivision of the slag into 16 layers extending from the surface of the slag to the matte layer, the resistances of these layers were evaluated with the use of the Attwood expression (4) x ½ and equation (5) (Table I). The resistance for the single electrode is predicted to be 8.5 mΩ compared with a furnace value of 10.2 mΩ, if an average immersion depth of 0.4 m is assumed. However, the slag temperature was higher than usual, implying that the electrode would be riding high.

Table I. Calculation of the Furnace Resistance

Depth of Slag, m	Avg. Temp. °C	Resistivity Ωm	$k_{Attwood}$ m^{-1}	$k_{Eqn.\ (5)}$ m^{-1}	Resistance mΩ	
0.1	1350	0.532	0.2658		141.4	
0.2	1490	0.328	0.2658		87.45	
0.3	1490	0.329	0.2658		87.45	
0.4	1485	0.335	0.2658		84.05	
0.5	1457	0.368		0.00683	2.51)	
0.6	1447	0.381		0.00474	1.806)	
0.7	1440	0.390		0.00363	1.416)	
0.8	1432	0.398		0.00294	1.17)	
0.9	1425	0.407		0.00248	1.01)	
1.0	1417	0.418		0.00213	0.89)	R
1.1	1412	0.425		0.00188	0.80)	
1.2	1403	0.438		0.00168	0.735)	
1.3	1393	0.454		0.00152	0.688)	
1.4	1382	0.470		0.00138	0.65)	
1.5	1369	0.489		0.00127	0.62)	
1.6	1305	0.760		0.00117	0.892)	

R_T = total furnace resistance R = 13.19 mΩ

Then $$\frac{1}{R_T} = \frac{1}{141.4} + \frac{1}{87.45} + \frac{1}{87.45} + \frac{1}{84.05} + \frac{1}{13.19}$$

$$R_T = 8.5\ m\Omega$$

Taking the average resistivity of the slag and integrating between 0 and h, equation (5) simplifies to:

$$k = \frac{4h}{\pi(S^2 - D^2)} \ln \frac{S^2}{D^2} \qquad \ldots\ldots\ldots\ldots\ldots\ldots (6)$$

that depends only on the distance of the electrode tip from the matte layer, and gives a resistance of 13.7 mΩ, compared with 13.2 mΩ.

Figure 1[4] shows/...

Figure 14 shows the variation of electrode to bath resistance for different electrode-immersion depths and the predicted values based on equations (4) and (6). The agreement is remarkable when the assumptions made are considered. The furnace resistance would be greater owing to the erosion around the electrode tip, which would decrease its effective diameter.

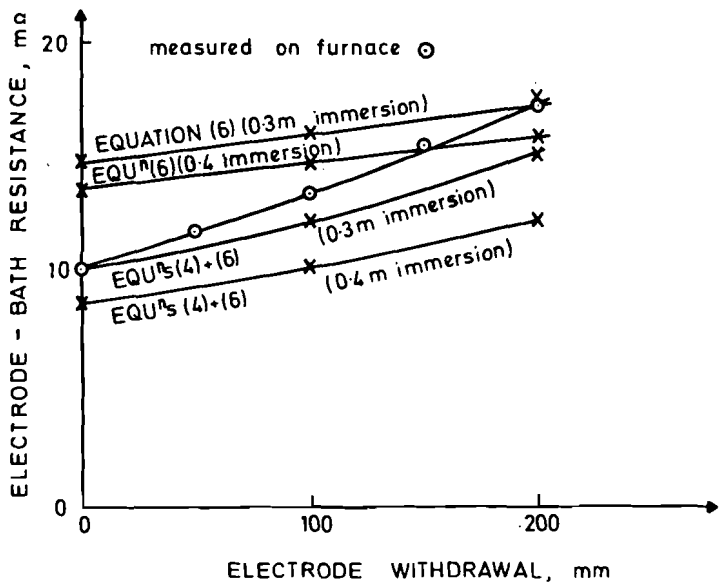

FIGURE 14 Variation in furnace resistance

For determination of the furnace dimensions, it would be necessary to know the heat-flow characteristics around each electrode, based on conduction, convection, and current density. However, based on a figure of 65 per cent backmix volume, as measured by the tracer experiments, it is assumed that there is a cylindrical reaction zone around each electrode having the same height as the slag layer. This gives a reaction zone diameter of 5.8 m compared with a furnace width of 7 m, and a settling region of 2.7 m. Tracer tests at different power levels and in different furnaces should make it possible to build up a reliable model.

Conclusions

The furnace investigations showed that the slag was very homogeneous except at either end of the furnace where there was an increase in concentration of chromium oxide at the slag-matte interface. This increase was shown to originate from the local ore. Radioactive tracer

tests confirmed/...

tests confirmed that the slag was very well mixed along the length of the furnace, about 65 per cent of the slag volume being accounted for by backmix. The tests offered a means of comparison of the flow conditions in the reverberatory and electric furnaces. Model experiments gave insight into the mode of current flow and power distribution within the furnace. The model experiments and actual furnace measurements enabled a cell constant to be derived for the calculation of the furnace resistance, which was in reasonable agreement with the actual operation.

Acknowledgements

This paper is published by permission of the Director General of the National Institute for Metallurgy, Johannesburg, and Johannesburg Consolidated Investment Company.

References

1. Mostert, J.C. and Roberts, P.N. "Electric smelting at Rustenburg Platinum Mines Limited of copper-nickel concentrates containing platinum-group metals", J.S. Afr. Inst. Min. Metall., Vol. 73, No. 9, 1973, pp. 290-299.

2. Themelis, N.J. and Spira, P. "Flow phenomena in reverberatory smelting", Trans. Metall. Soc. AIME, Vol. 236, 1966, pp.821-828.

3. Hejja, A.A. "Viscosities and electrical conductivities of slags: Application to the study of characteristics and performance of electric matte smelting furnaces", Progress Report No. 2, Department of Metallurgy, University of the Witwatersrand, Johannesburg, Nov. 9, 1973.

4. Themelis, N.J. "Techniques of process analysis in extractive metallurgy", Metall. Trans., Vol. 3, Aug. 1972, pp. 2021-29.

5. Barth, O. "Electric smelting of sulphide ores", Extractive Metallurgy of Copper, Nickel and Cobalt, Ed. P. Queneau, Interscience Publishers, New York, 1961.

6. Tseidler, A.A. "Metallurgy of copper and nickel", Israel Program for Scientific Translations Ltd, Keter Press, Jerusalen, 1964, p. 266.

7. Channon, W.P. Urquhart, R.C. and Howat, D.D. "The mode of current transfer between electrode and slag in the submerged-arc furnace", J.S. Afr. Inst. Min. Metall., Vol. 75, Aug. 1974, pp. 4-7.

8. Persson, J.A. and Treilhard, D.G. "Electrothermic smelting of copper and nickel sulphides and other metal bearing constituents", J. of Metall. AIME, Jan. 1973, pp. 34-39.

Reference 9/...

9. Attwood, S.S. Electric and magnetic fields, J. Wiley, New York, 1949, p. 88.

10. Hallvard-Nilsen, P. "Determination of the electrical resistance in idealized-resistance furnaces from model experiments", Tids. Kjemi. Bergv. Metall., Vol. 21, No. 2, 1961, pp. 27-33.

Document Summary

for "The Smelting of Copper-Nickel Concentrates in an Electric Furnace"

< Back

BOOKMARK

Title	**The Smelting of Copper-Nickel Concentrates in an Electric Furnace** View Document
Author	Urquhart, Roger C.
Society / Organization	TMS
Summary / Abstract	Copper-nickel-sulphide ores mined in the Rustenburg district of South Africa are generally smelted in electric furnaces because of the high-temperature slag produced, the availability of cheap electric power, and the smaller pollution problems. Apart from melting, the functions of the electric furnace are to recover most of the matte content in the converter slag by physical and chemical interaction with the furnace bath and to provide adequate time for the optimum separation of matte and slag. Smooth, efficient operation will denend on fluid slags for settling, balanced by high resistivities to obtain adequate concentration and distribution of power by way of current heating. To obtain a greater understanding of the processes involved, an investigation was undertaken at Rustenburg Platinum Mines on the smelting of copper-nickel concentrates in a 19.5 MVA furnace with six in-line electrodes. The matte- and slag-tapping temperatures, slag temperatures, slag analyses, electrical data, and electrode position were measured. Radioactive tracers were introduced into the slag, and quantitative results relating to the flow pattern within the furnace were obtained. These studies were augmented by scaled laboratory investigations relating to the determination of cell constants and current distribution within the furnace. Instantaneous field and power distribution plots were determined by use of an on-line mini-computer. The applicability of these results to furnace operation is discussed.
Format	PDF
File Size	387.9k
Specifications	v 9.0 / 300 dpi
Copyright Date	1/1/76
Publication Date	1/1/76
Digitization Date	1/28/11
Book Title	Extractive Metallurgy of Copper (1976) Volume I
Chapter	14 - Copper Smelting Slags
Pages	22